NJC

Accepted Manuscript

This article can be cited before page numbers have been issued, to do this please use: C. Bustos, E. Molins, J. Carcamo, M. Aguilar, C.O. Sánchez, I. Moreno-Villoslada, H. Nishide, X. Zarate and E. Schott, *New J. Chem.*, 2015, DOI: 10.1039/C5NJ02604K.

This is an *Accepted Manuscript*, which has been through the Royal Society of Chemistry peer review process and has been accepted for publication.

Accepted Manuscripts are published online shortly after acceptance, before technical editing, formatting and proof reading. Using this free service, authors can make their results available to the community, in citable form, before we publish the edited article. We will replace this *Accepted Manuscript* with the edited and formatted *Advance Article* as soon as it is available.

You can find more information about *Accepted Manuscripts* in the Information for Authors.

Please note that technical editing may introduce minor changes to the text and/or graphics, which may alter content. The journal's standard Terms & Conditions and the Ethical guidelines still apply. In no event shall the Royal Society of Chemistry be held responsible for any errors or omissions in this *Accepted Manuscript* or any consequences arising from the use of any information it contains.

View Article Online
DOI: 10.1039/C5NJ02604K

A family of substituted hydrazonoisoxazolones with potential biological properties

Carlos Bustos[a,*], Elies Molins[b], Juan-Guillermo Cárcamo[c], Marcelo N. Aguilar[c], Christian Sánchez[a], Ignacio Moreno-Villoslada[a], Hiroyuki Nishide[d], Ximena Zarate[e] and Eduardo Schott[f,*]

[a]*Instituto de Ciencias Químicas, Universidad Austral de Chile, Las Encinas 220, Campus Isla Teja, Valdivia, Chile.*

[b]*Institut de Ciència de Materials de Barcelona (ICMAB-CSIC), Campus de la Universitat Autònoma de Barcelona, 08193 Bellaterra, Spain.*

[c]*Instituto de Bioquímica y Microbiología, Universidad Austral de Chile, Campus Isla Teja, Valdivia, Chile.*

[d]*Department of Applied Chemistry, School of Science and Engineering, Waseda University, Tokyo 169-8555, Japan.*

[e]*Instituto de Ciencias Químicas Aplicadas, Facultad de Ingeniería, Universidad Autónoma de Chile, Av. Pedro de Valdivia 641, Santiago, Chile.*

[f]*Departamento de Química Inorgánica, Facultad de Química, Pontificia Universidad Católica de Chile, Avda. Vicuña Mackenna 4860, Santiago, Chile*

*email: maschotte@gmail.com, Phone/Fax: (562)-2354-1422.

Keywords: 3,4-R-Isoxazolones, Organic synthesis, Antiproliferative, Cytitoxic effect, X-Ray

Abstract

The synthesis, characterization and biological study of a new 3,4,5-trisubstituted isoxazolones have been reported. In this sense a series of (*Z*)-3-methyl-4-(2-(R-phenyl)hydrazinylidene)isoxazol-5(4*H*)-ones were prepared by reaction of a β-diketohydrazone with hydroxilammonium chloride. All products were characterized using EA, UV-Vis, FT-IR, ^{1}H-NMR, ^{13}C-NMR spectroscopy and HMBC. The crystalline and molecular structure of three compounds were solved by X-Ray diffraction methods. Density functional theory (DFT) and Time-dependent DFT (TDDFT) calculations were performed to give a better explanation of the observed experimental behaviour of

View Article Online
DOI: 10.1039/C5NJ02604K

these newly synthetized compounds. Furthermore, the report of cytotoxicity and the antiproliferative effect in human *promielocytic leukemia* cells, HL-60 was tested by the MTT reduction method, showing most of the newly synthetized compounds important antineoplastic activity. The most active isoxazolones were used in experiments of reverse transcription polymerase chain reaction (RT-PCR) to determine the effect on the expression levels on *m*RNA encoding using the anti-apoptotic, Bcl 2, pro-apoptotic, Bax, and the proliferation inhibition $p21^{WAF-1}$ proteins. Therefore, it was possible to fully characterize the complete library of 15 isoxazolones and to show that most of them are antineoplastic trough an apoptotic pathway.

INTRODUCTION

The biological activity of substituted isoxazoles has made them an interesting focus for medicinal chemistry in the last years[1]. In fact, isoxazoles are potent, selective agonists at human cloned dopamine D4 receptor[2] and exhibit $GABA_A$ antagonist[3], analgesic[4], antiinflamatory[4], ulcerogenic[4], antimicrobial[5], antifungal[5], COX-2 inhibitory[6,7], antinociceptive[8] and anticancer[9] activity.

Many synthetic methods have been employed to obtain substituted isoxazoles including reactions of hydroxilamine with 1,3-dicarbonyl compounds[10], α,β-unsaturated carbonyl compounds[11] and α,β−unsaturated nitriles[12]. The reaction of an oxime-derivative dianion with esters[13] or amides[14,15] also yields isoxazoles. On the other hand, [3+2] cycloaddition reactions of alkynes and nitrile oxides have also been developed[16]. However, these methods often require strong bases, strong mineral acids, high temperatures or they provide poor regioselectivity. Isoxazoles can be also halogenated to give substituted haloisoxazoles[17], however under the reaction conditions high temperatures are required.In this work we report a one-pot synthesis of isoxazolones, of the type (Z)-3-methyl-4-(2-(R-phenyl)hydrazinylidene)isoxazol-5(4H)-ones. These compounds were obtained by cyclization of an *in situ* generated oxime, formed by reaction of (*E*)-ethyl 2-(2-(R-phenyl)hydrazinylidene)-3-

View Article Online
DOI: 10.1039/C5NJ02604K

oxobutanoates with hydroxilammonium chloride in acid media (R= *4*-OH(**1**), *4*-CH_3(**2**), *4*-OCH_3(**3**), *4*-H(**4**), *4*-Cl(**5**), *4*-Br(**6**), *4*-CO_2H(**7**), *4*-$COCH_3$(**8**), *4*-CN(**9**), *4*-NO_2(**10**), *2*-OH (**11**), 2-Cl(**12**), *2*-CO_2H(**13**), *2*-NO_2(**14**), *3*-Cl(**15**)). Besides, we present the spectroscopic characterization and structures of three representative compounds. Finally, considering that numerous isoxazole derivatives have shown biological activity, we perform a study of antitumor activity in order to evaluate the cytotoxic activity of these compounds towards the human promyelocytic leukemia cell line, HL-60[18–22]. Besides, using compounds with IC_{50} values lower than 83 μM, we performed reverse transcription polymerase chain reaction (RT-PCR) experiments to determine the effect on the expression levels of mRNA codifying for anti- and pro-apoptotic genes, Bcl-2 and Bax, and a gene involved in the inhibition of cell cycle progression, $p21^{WAF-1}$.

EXPERIMENTAL

Chemicals

Substituted anilines (R-C_6H_4-NH_2 R= *4*-OH(**1**), *4*-CH_3(**2**), *4*-OCH_3(**3**), *4*-H(**4**), *4*-Cl(**5**), *4*-Br(**6**), *4*-CO_2H(**7**), *4*-$COCH_3$(**8**), *4*-CN(**9**), *4*-NO_2(**10**), *2*-OH (**11**), 2-Cl(**12**), *2*-CO_2H(**13**), *2*-NO_2(**14**), *3*-Cl(**15**)), acetylacetone, sodium nitrite, hydrochloric acid, sodium hydroxide, hydroxilammonium chloride and acetic acid were procured from Sigma-Aldrich Corporation and the solvents (methanol, ethanol, diethylether, acetone *$CDCl_3$*, and *DMSO-d_6*) from commercial sources including Merck, Fisher and T. J. Baker providers. All β-diketohydrazone precursors, were obtained as previously as described in literature[23] and the structures were checked by IR spectroscopy and, in some cases, by ^{1}H NMR spectroscopy.

Physical measurements

View Article Online
DOI: 10.1039/C5NJ02604K

Uncorrected melting points, MP, were determined on a digital STUARD, SMP10 apparatus. The elemental analysis were obtained in a FISONS, EA 1118 microanalyser using sulfanilamide as standard. UV-visible spectra were recorded in the 1100-200 nm range, in quartz cells with 10 mm length pass, using a Perkin Elmer, Lambda 35 spectrophotometer, diluting the concentrated solutions, ~1.0×10^{-3} mole/L of each compound to around ~1.0×10^{-3} mole/L. The infrared spectra, IR, were obtained in solid state on a *Jasco* ATR PRO450-S, mounted on a *Jasco* FT/IR-4200 equipment. Depending on the solubility of compounds, the ^{1}H NMR, ^{13}C NMR and HMBC spectra were recorded by the standard methods in $CDCl_3$ or *DMSO-*d_6 solutions, using 5 mm i.d. glass tubes and the internal solvent signals as reference in two different equipment i) JOEL, JNM-Lambda500 spectrophotometer and ii) a Bruker, Avance AM 400 spectrophotometer. Assignment of ^{1}H and ^{13}C NMR signals was realized according to Figure 1.

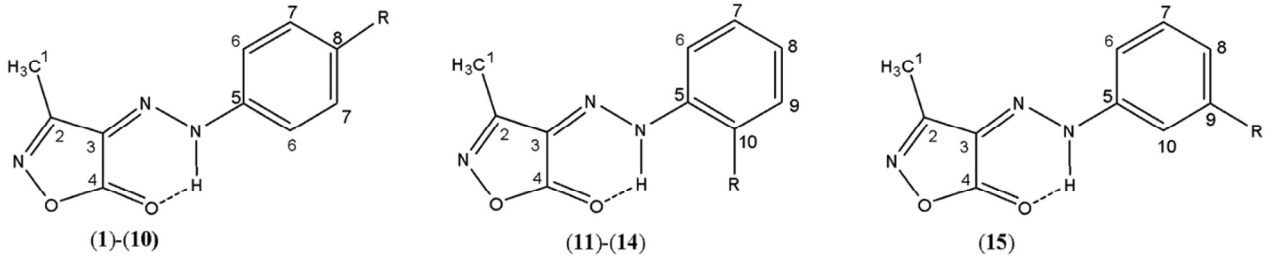

Figure 1. Numeration used for ^{1}H- and ^{13}C-NMR assignation.

Crystallography

Highly redundant single crystals X-ray diffraction data set of **4**, **12** and **15** were collected at room temperature up on a Bruker AXS SMART APEX CCD diffractometer using monochromatic MoKα radiation, λ= 0.71069 Å, and a 0.3º separation between frames. Data collection of crystals and refinement of structures are shown in Table 1, while Table S1 contains the selected bond lengths and angles and Figures 2 exhibit an ORTEP view of each molecule. Data integration was performed using SAINT program contained in the diffractometer package. The structures were solved by direct

View Article Online
DOI: 10.1039/C5NJ02604K

methods and Fourier's difference maps were refined by least squares on F^2 with anisotropic displacement parameters for non-H atoms. All hydrogen atoms were located from difference Fourier maps and refined isotropically. All calculations to solve the structure and to refine the model proposed and to obtain results were carried out with the computer programs SHELXS-97 and SHELXL-97 and SHELXTL/PC[24]. Crystallographic data (excluding structure factors) for the structures reported in this paper have been deposited in the Cambridge Crystallographic Data Centre as supplementary publication, No. 1062571 for compound (**12**) and 1062570 for compound (**15**). Copies of this information may be obtained free of charge from The Director, CCDC, 12 Union Road, Cambridge CB2 1EZ, UK. Fax: +44 1223 336 033. E-mail: data_request@ccdc.cam.ac.uk. Web page: http://www.ccdc.cam.ac.uk. In case of compound 4 a previous report was found. However the crystallization methodology is different. In this case the ethanol was allowed to slowly evaporate from the solution. The obtained X-Ray for **4** is reported in the supplementary information and for comparison see Bertolasi et. al.[25].

Table 1. Crystal data and structure refinement of compounds **4**, **12** and **15**.

Compound	**4**	**12**	**15**
Empirical formula	$C_{10}H_9N_3O_2$	$C_{10}H_8ClN_3O_2$	$C_{10}H_8N_3O_2Cl$
Formula weight (g/mol)	203.2	237.64	237.64
Temperature (K)	294(2)	294(2) K	294(2)
Wavelength (Å)	0.71073	0.71073	0.71073
Crystal system	Monoclinic	Triclinic	Monoclinic
Space group	C2/1	$P\bar{1}$	$P2_1/c$
Unit cell dimension (Å), (º)	a= 11.117(4), α= 90 b= 7.955(2), β= 95.76(2) c= 21.817(4), γ= 90	a=7.642(2), α=98.77 b=7.933(2), β=104.53 c=9.511(1), γ=98.06	a= 12.577(3), α= 90 b=8.509(8), β= 102.90(2) c=20.565(6), γ= 90
Volume ($Å^3$)	1919.9(9)	541.9(2)	2145(2)
Z	8	2	8
Density (Mg/m^3)	1.406	1.456	1.472
Absorption coefficient (mm^{-1})	0.102	0.34	0.344

View Article Online
DOI: 10.1039/C5NJ02604K

F(000)	848	244	976
Crystal size (mm^3)	0.41×0.38×0.32	0.42×0.27×0.09	0.47×0.45×0.15
θ range for data collection(º)	1.88-25.97	2.26 to 27.95	1.66-25.98.
Index ranges	$-13 \le h \le 13$ $0 \le k \le 9$ $0 \le l \le 26$	$-10 \le h \le 9$ $-10 \le k \le 10$ $0 \le l \le 12$	$-15 \le h \le 15$ $0 \le k \le 10$ $0 \le l \le 25$
Reflections collected	1893	5299	4213
Independent reflections	1893	2605	4213
Completeness to θ (%)	100	100	100
Max and Min. Transmission	0.9681 and 0.9594	0.8477 and 0.9699	0.9502 and 0.8551
Refinement method	Full-matrix least-squares on *F2*	Full-matrix least-squares on *F2*	Full-matrix least-squares on *F2*
Data/restrain/parameters	1893/0/122	2605/0/150	4213/0/291
Goodness-of-fit on F^2	0.981	0.913	1.009
Final R indices [$I>2\sigma(I)$]	*R1* = 0.0459, *wR2* = 0.0989	*R1* = 0.0497, *wR2* = 0.1158	*R1* = 0.0615, *wR2* = 0.1297
R indices (all data)	*R1* = 0.1056, *wR2* = 0.1120	*R1* = 0.1192, *wR2* = 0.1376	*R1* = 0.1267, *wR2* = 0.1462
Largest diff. Peak/hole (e×Å^{-3})	0.149/-0.219	0.210 and -0.160	0.197/-0.287

Synthesis. In a 100 mL round-bottomed flask were added 0.01 mmole of any β-diketohydrazone, R-C_6H_4-NHN=C($COCH_3$)($CO_2CH_2CH_3$), Scheme 1, {R= *4*-OH(**1**), 2.62 g; *4*-CH_3(**2**), 2.60 g; *4*-OCH_3(**3**), 2.76 g; *4*-H(**4**), 2.46 g; *4*-Cl(**5**), 2.81 g; *4*-Br(**6**), 3.25 g; *4*-CO_2H(**7**), 2.90 g; *4*-$COCH_3$(**8**), 2.88 g; *4*-CN(**9**), 2.71 g; *4*-NO_2(**10**), 2.91 g; *2*-OH (**11**), 2.62 g; 2-Cl(**12**), 2.81 g; *2*-CO_2H(**13**), 2.90 g; *2*-NO_2(**14**), 2.91 g; *3*-Cl(**15**), 2.81 g} 25 mL of ethanol, 2 mL of glacial acetic acid and 0.01 mol (0.69 g) of $NH_2OH·HCl$. The reaction mixture was stirred and heated at reflux during 18 h. Then the partially precipitated solution was cooled at -18 ºC by 4 h and the red-yellow solid was filtered by suction, washed with 100-200 mL of water and dried at 40 ºC in a vacuum oven by 24 h. All products were recrystallized from ethanol, where compounds **4**, **12** and **15** yield single crystals suitable for diffractometric studies

Analysis

View Article Online
DOI: 10.1039/C5NJ02604K

The corresponding spectra for I.R., ^{1}H-NMR, ^{13}C-NMR and HBMC are included in the supplementary information for each of the synthetized compounds. A summary of the obtained results are shown here.

(Z)-4-(2-(4-hydroxyphenyl)hydrazono)-3-methylisoxazol-5(4H)-one (**1**)**:** Crude yield: 35.6%. Final Yield: 22.5% MP ºC: 211-212. Anal. Calc. (%) for $C_{10}H_9N_3O_3$ **(**Mι: 219,20 g/mol: C, 54.79; H, 4.14; N, 19.17; Found (%): C, 54.57; H, 4.25; N, 18.98. UV-visible spectrum in ethanol solution 5×10^{-5} mol/L, λ_{max}, nm (log**ε**): 427(4.40); 296(2.72); 252(4.01); 201(4.12). I.R. spectrum in solid state, $\overline{\nu}$ (cm^{-1}); ν(O-H): 3187s; ν(C-H, aliph.): 2822w, 2684w, 2587w; ν(C=O): 1708s; ν(C=N): 1598m; ν(C=C): 1556m; ν(N-O): 1000w. ^{1}H NMR in *DMSO-d_6*, δ ppm: 2.23 (s, 3H), 6.81 (d, J = 9.01 Hz, 2H), 7.54 (d, *J* = 8.97 Hz, 2H), 9.76 (s, 1H), 12.80 (s, 1H). ^{13}C NMR in *DMSO-d_6*, δ ppm: 10.01, 116.02, 118.16, 118.68, 133.53, 156.50, 159.63, 163.05.

(Z)-3-methyl-4-(2-p-tolylhydrazono)isoxazol-5(4H)-one (**2**): Crude yield: 98.9%. Final Yield: 90% MP: 189-190 ºC. Anal. Calc. (%) for $C_{11}H_{11}N_3O_2$ (Mι: 217,22 g/mol): C, 60.82; H, 5.10; N, 19.34. Found (%): C, 60.74; H, 5.25; N, 19.72. UV-visible spectrum in ethanol solution 5×10^{-5} mol/L, λ_{max}, nm (log**ε**): 405 (3.37); 260 (3.94); 252(4.02); 232(4.03); 202(4.40). I.R. spectrum in solid state, $\overline{\nu}$ (cm^{-1}); ν(N-H): 3204s; ν(C-H, arom.): 3023w; ν(C-H, aliph.): 2978w, 2963w; 2924w, 2858w; ν(C=O): 1705s; ν(C=N): 1595w; ν(C=C): 1563s; ν(N-O): 993w. ^{1}H NMR in *$CDCl_3$,* δ ppm: 2.33 (s, 3H), 2.38 (s, 3H), 7.23 (d, *J* = 8.36 Hz, 2H), 7.32 (d, *J* = 8.51 Hz, 2H), 12.69 (s, 1H). ^{13}C NMR in *$CDCl_3$*, δ ppm: 10.34, 21.20, 116.25, 120.63, 130.52, 137.15, 138.30, 159.49, 165.30.

(Z)-4-(2-(4-methoxyphenyl)hydrazono)-3-methylisoxazol-5(4H)-one (**3**): Crude yield: 85.2%. Final Yield: 82.2% MP: 202-203 ºC. Anal. Calc. (%) for $C_{11}H_{11}N_3O_3$ (Mι :231,255 g/mol): C, 56.65; H,

View Article Online
DOI: 10.1039/C5NJ02604K

4.75; N, 18.02; Found (%): C, 56.45, H, 5.13, N, 17.97. UV-visible spectrum in ethanol solution 5×10^{-5} mol/L, λ_{max}, nm (log**ε**): 420(4.41); 301(3.41); 252(4.02); 201(4.26). I.R. spectrum in solid state, $\overline{\nu}$ (cm^{-1}); ν(N-H): 3189m; ν(C-H, arom.): 3083w, 3040w and 3015w; ν(C-H, aliph.): 2961w, 2932w, 2896w and 2834m; ν(C=O): 1703s; ν(C=N): 1593m; ν(C=C): 1554s; ν(N-O): 990w. ^{1}H NMR in *CDCl₃,* δ ppm: 2.32 (s, 3H), 3.85 (s, 3H), 6.97 (d, *J* = 9.08 Hz, 2H), 7.38 (d, *J* = 9.12 Hz, 2H), 12.78 (s, 1H). ^{13}C NMR in *CDCl₃*, δ ppm: 10.19, 55.64, 115.10, 117.63, 119.91, 134.01, 158.68, 159.28, 165.39.

(Z)-3-methyl-4-(2-phenylhydrazono)isoxazol-5(4H)-one (**4**): Crude yield: 87.1% Final Yield: 81.1% MP ºC: 185-186. Anal. Calc. (%) for $C_{10}H_9N_3O_2$ (Mı: 203,20 g/mol): C, 59.11; H, 4.46; N, 20.68; Found (%): C, 58.99; H, 4.76; N, 20.67. UV-visible spectrum in ethanol solution 5×10^{-5} mol/L, λ_{max}, nm (log**ε**): 396(4.40); 255(4.00); 249(4.05); 200(4.05). I.R. spectrum in solid state, $\overline{\nu}$ (cm^{-1}); ν(N-H): 3207s, ν(C-H, arom.): 3118w, 3056w and 3031w; ν(C-H, aliph.): 2978w, ν(C=O): 1709s; ν(C=N): 1594w; ν(C=C): 1572sh and 1561w; ν(N-O): 991w. ^{1}H NMR in *CDCl₃*, δ ppm: 2.34 (s, 3H), 7.34-7.18 (m, 1H), 7.46-7.40 (m, 4H), 12.67 (s, 1H). ^{13}C NMR in *CDCl₃*, δ ppm: 10.20, 116.12, 121.18, 126.75, 129.82, 140.40, 159.39; 164.95.

(Z)-4-(2-(4-chlorophenyl)hydrazono)-3-methylisoxazol-5(4H)-one (**5**): Crude yield: 99.2%. Final Yield: 95.7% MP ºC: 184-185 ºC. Anal. Calc.(%) for $C_{10}H_8ClN_3O_2$ (Mı: 237,64 g/mol): C, 50.54; H, 3.39; N, 17.68; Found (%): C, 50.26; H, 3.46; N, 17.55. UV-visible spectrum in ethanol 5×10^{-5} mol/L, λ_{max}, nm (log**ε**): 397(4.43); 296(3.35); 250(4.06); 200(4.15). I.R. spectrum in solid state, $\overline{\nu}$ (cm^{-1}); ν(N-H): 3206s; ν(C-H, arom.): 3101w; 3093w, 3077w, 3070w; ν(C-H, aliph.): 2927w; ν(C=O): 1715s; ν(C=N): 1593w; ν(C=C): 1552s; ν(N-O): 993m. ^{1}H NMR in *CDCl₃,* δ ppm: 2.33 (s,

View Article Online
DOI: 10.1039/C5NJ02604K

3H), 7.36 (d, J = 8.75 Hz), 7.41 (d, J = 8.75 Hz, 2H), 12.64 (s, 1H). ^{13}C NMR in *CDCl$_3$*, δ ppm: 10.21; 117.22, 121.81, 129.97, 132.04, 139.03, 159.28, 164.84.

(Z)-4-(2-(4-bromophenyl)hydrazono)-3-methylisoxazol-5(4H)-one (**6**): Crude yield: 69.2%. Final Yield: 62.4% MP 194-195 ºC. Anal. Calc. (%) for $C_{10}H_8BrN_3O_2$ (Mɪ: 282,09g/mol): C, 42.58; H, 2.86; N, 14.90; Found (%): C, 42.47; H, 3.02; N, 14.70. UV-visible spectrum in ethanol solution 5× 10^{-5} mol/L, λ_{max}, nm (log**ε**): 399(4.45); 296(2.28); 251(4.05); 201(4.19). I.R. spectrum in solid state, $\overline{\nu}$ (cm^{-1}); ν(N-H): 3206s; ν(C-H, arom.): 3097w, 3069w and 3011w; ν(C-H, aliph.): 2926w; ν(C=O): 1715s; ν(C=N): 1591w; ν(C=C): 1559s; ν(N-O): 992w. ^{1}H NMR in *CDCl$_3$*, δ ppm: 2.33 (s, 3H), 7.30 (d, J = 2.13 Hz, 2H), 7.56 (d, J = 2.13 Hz, 2H), 12.62 (s, 1H). ^{13}C NMR in *CDCl$_3$*, δ ppm: 10.20, 117.51, 119.72, 121.92, 132.89, 139.50, 159.29, 164.82.

(Z)-4-(2-(3-methyl-5-oxoisoxazol-4(5H)-ylidene)hydrazinyl)benzoic acid (**7**): Crude yield: 63.1%. Final Yield: 58.5% MP dec. at 226 ºC. Anal. Calc. (%) for $C_{11}H_9N_3O_4$ (Mɪ : 247,21 g/mol): C, 53.44; H, 3.67; N, 17.00; Found (%): C, 53.57; H, 4.86; N, 16.88. UV-visible spectrum in ethanol solution 5× 10^{-5} mol/L, λ_{max}, nm (log**ε**): 396(4.51); 256(4.08); 211(3.97); 201(4.14). I.R. spectrum in solid state, $\overline{\nu}$ (cm^{-1}); ν(N-H): 3200w, ν(O-H): 3400-2200 range; ν(C=O): 1714s and 1673s; ν(C=N): 1606m; ν(C=C): 1556s; ν(N-O): 997w. ^{1}H NMR in *DMSO-d$_6$*, δ ppm: 2.26 (s, 3H), 7.75 (dd, J = 4.69, 2.13 Hz, 2H), 7.99 (dd, J = 4.69, 2.13 Hz, 2H), 12.78 (s, 1H), 12.92 (s, 1H). ^{13}C NMR in *DMSO-d$_6$*, δ ppm: 9.99, 116.37, 122.05, 127.55, 130.73, 144.86, 159.97, 161.88, 166.58.

(Z)-4-(2-(4-acetylphenyl)hydrazono)-3-methylisoxazol-5(4H)-one (**8**): Crude yield: 93.4%. Final Yield: 87.5% MP 198-199 ºC. Anal. Calc. (%) for $C_{12}H_{11}N_3O_3$ (Mɪ: 245,23 g/mol): C, 58.77; H,

View Article Online
DOI: 10.1039/C5NJ02604K

4.52; N, 17.13; Found (%) C, 58.57; H, 4.35; N, 16.99. UV-visible spectrum in ethanol solution 5 10^{-5} mol/L, λ_{max}, nm (log**ε**): 399(4.41); 276(3.89); 254(3.77); 246(3.79); 201(4.31). I.R. spectrum in solid state, $\overline{\nu}$ (cm^{-1}); ν(N-H): 3207w; ν(C-H, arom.): 3097w, 3060w, and 3002w; ν(C-H, aliph.): 2925w; ν(C=O): 1712s and 1678s; ν(C=N): 1601w and 1591w; ν(C=C): 1564w; ν(N-O): 996w. ^{1}H NMR in *$CDCl_3$,* δ ppm: 2.36 (s, 3H), 2.62 (s, 3H), 7.48 (d, *J* = 8.76 Hz, 2H), 8.05 (d, *J* = 8.76 Hz, 2H), 12.65 (s, 1H). ^{13}C NMR in *$CDCl_3$*, δ ppm: 10.23, 26.51, 115.72, 123.22, 130.35, 134.82, 143.87, 159.35, 164.41, 196.39.

(Z)-4-(2-(3-methyl-5-oxoisoxazol-4(5H)-ylidene)hydrazinyl)benzonitrile (**9**): Crude yield: 96.4%. Final Yield: 91.3% MP ºC: 185-186. Anal. Calc. (%) for $C_{11}H_8N_4O_2$ (Mı: 228,21g/mol) C, 57.89; H, 3.53; N, 24.55; Found (%): C, 57.70; H, 3.79; N, 24.12. UV-visible spectrum in ethanol solution 2.5 $\times 10^{-5}$ mol/L, λ_{max}, nm (log**ε**): 391(4.50); 254(4.09); 201(4.15). I.R. spectrum in solid state, $\overline{\nu}$ (cm^{-1}); ν(N-H): 3210s; ν(C-H, arom.): 3091w 3064w; ν(C-H, aliph.): 2970w; ν(C≡N): 2223s; ν(C=O): 1720s; ν(C=N): 1589s; ν(C=C): 1560s; ν(N-O): 993m. ^{1}H NMR in *$CDCl_3$,* δ ppm: 2.36 (s, 3H), 7.52 (d, *J* = 8.78 Hz, 2H), 7.74 (d, *J* = 8.75 Hz, 2H), 12.59 (s, 1H). ^{13}C NMR in *$CDCl_3$*, δ ppm: 10.22, 109.34, 116.23, 118.20, 124.01, 133.94, 143.66, 159.26, 164.13.

(Z)-3-methyl-4-(2-(4-nitrophenyl)hydrazono)isoxazol-5(4H)-one (**10**): Crude yield: 97.9%. Final Yield: 91.2% MP ºC: 177-178. Anal. Calc. (%) for $C_{10}H_8N_4O_4$ (Mı: 248,19 g/mol): C, 48.39; H, 3.25; N, 22.57; Found (%): C, 42.81; H, 3.51; N, 22.58. UV-visible spectrum in ethanol solution 2.5 $\times 10^{-5}$ mol/L, λ_{max}, nm (log**ε**): 400(4.59); 297(3.74); 222(3.99); 202(4.20). I.R. spectrum in solid state, $\overline{\nu}$ (cm^{-1}); ν(N-H): 3205s; ν(C-H, arom.): 3108w, 3092 and 3009w; ν(C-H, aliph.): 2933w; ν(C=O): 1720s ν(C=N): 1611w; ν(C=C): 1557s; ν(N-O): 994m. ^{1}H NMR in *DMSO-d_6*, δ ppm: 2.27

View Article Online
DOI: 10.1039/C5NJ02604K

(s, 3H), 7.86 (d, *J* = 9.27 Hz, 2H), 8.29 (d, *J* = 9.26 Hz, 1H), 12.85 (s, 1H). ^{13}C NMR in *DMSO-d*$_6$, δ ppm: 10.02, 116.86, 123.83, 125.28, 143.96, 146.87, 160.07, 161.30.

(Z)-4-(2-(2-hydroxyphenyl)hydrazono)-3-methylisoxazol-5(4H)-one (**11**): Crude yield: 80.0%. Final Yield: 71.4% MP: 209-210 ºC. Anal. Calc. (%) for $C_{10}H_9N_3O_3$ (Mt: 219,20 g/mol): C, 54.79; H, 4.14; N, 19.17; Found (%): C, 52.89; H, 4.68; N, 18.08. UV-visible spectrum in ethanol solution 2.5×10^{-5} mol/L, λ_{max}, nm (log**ε**): 425(4.36); 245(3.91); 202(4.13). I.R. spectrum in solid state, $\bar{\nu}$ (cm^{-1}); ν(N-H): 3194w; ν(O-H): 3400-2400 range; ν(C=O): 1717s; ν(C=N): 1599w; ν(C=C): 1536s; ν(N-O): 1001m. ^{1}H NMR in *DMSO-d*$_6$, δ ppm: 2.26 (s, 3H), 6.94 (dd, *J* = 7.48, 1.26 Hz, 1H), 6.98 (d, *J* = 8.12,1H), 7.11 (dd, *J* = 7.43, 1.58 Hz, 1H), 7.60 (d, J = 8.07, 1H), 10.79 (s, 1H), 12.75 (s, 1H). ^{13}C NMR *DMSO-d*$_6$, δ ppm: 9.76, 114.62, 115.84, 120.22, 120.60, 127.04, 128.26, 146.30, 159.24, 164.19.

(Z)-4-(2-(2-chlorophenyl)hydrazono)-3-methylisoxazol-5(4H)-one (**12**): Crude yield: 96.3%. Final Yield: 85.6% MP: 165-166 ºC. Anal. Calc. (%) for $C_{10}H_8ClN_3O_2$ (Mt: 237,64 g/mol): C, 50.54; H, 3.39; N, 17.68; Found (%): C, 50.24; H, 3.54; N, 17.55. UV-visible spectrum in ethanol solution 2.5×10^{-5} mol/L, λ_{max}, nm (log**ε**): 395(4.20); 260(3.71); 252(3.80); 202(4.04). I.R. spectrum in solid state, $\bar{\nu}$ (cm^{-1}); ν(N-H): 3204m; ν(C-H, arom.): 3090w, 3067w and 3025w; ν(C-H, aliph.): 2928w; ν(C=O): 1719s; ν(C=N): 1595w and 1586w; ν(C=C): 1556s; ν(N-O): 991w. ^{1}H NMR in *CDCl*$_3$, δ ppm: 2.35 (s, 3H), 7.18 (dd, *J* = 7.99, 1.46 Hz, 1H), 7.37 (t, *J* = 7.82, 1H), 7.44 (d, *J* = 8.05, 1H), 7.79 (d, *J* = 8.25, 1H), 12.95 (s, 1H). ^{13}C NMR *CDCl*$_3$, δ ppm: 10.27, 116.13, 122.090, 123.33, 126.74, 128.26, 130.00, 137.07, 159.23,164.37. **4**

View Article Online
DOI: 10.1039/C5NJ02604K

(Z)-2-(2-(3-methyl-5-oxoisoxazol-4(5H)-ylidene)hydrazinyl)benzoic acid (**13**): Crude yield: 99.2%. Final Yield: 95.7% MP: 220-221 ºC. Anal. Calc. (%) for $C_{11}H_9N_3O_4$ (Mɪ: 247,21 g/mol): C, 53.44; H, 3.67; N, 17.00; Found (%): C, 53.49; H, 3.82; N, 16.87. UV-visible spectrum in ethanol solution 2.5×10^{-5} mol/L, λ_{max}, nm (log**ε**): 399(4.42); 264(3.98); 226(4.08); 206(4.30). I.R. spectrum in solid state, $\overline{\nu}$ (cm^{-1}); ν(O-H): 3300-2300 range; ν(C=O): 1733s and 1675s; ν(C=N): 1603m and 1586w; ν(C=C) 1551s; ν(N-O): 994s. ^{1}H NMR in *CDCl₃*, δ ppm: 2.26 (s, 3H), 7.30 (dd, *J* = 7.46, 1.03 Hz, 1H), 7.70 (dd, *J* = 7.39, 1.19 Hz, 1H), 7.92 (d, *J* = 8.23 Hz, 1H), 7.99 (d, *J* = 7.91, 1H). ^{13}C NMR in *CDCl₃*, δ ppm: 9.91, 115.02, 116.02, 122.99, 124.90 , 131.26, 134.53, 142.55, 159.659, 162.13, 168.23.

(Z)-3-methyl-4-(2-(2-nitrophenyl)hydrazono)isoxazol-5(4H)-one (**14**): Crude yield: 97.1%. Final Yield: 90.2% MP: 180-181 ºC. Anal. Calc. (%) for $C_{10}H_8N_4O_4$ (Mɪ: 248,19 g/mol): C, 48.39; H, 3.25; N, 22.57; Found (%): C, 48.45; H, 3.36; N, 22.45. UV-visible spectrum in ethanol solution 2.5×10^{-5} mol/L, λ_{max}, nm (log**ε**): 410(4.32); 344(4.09); 281(3.99); 201(4.38). I.R. spectrum in solid state, $\overline{\nu}$ (cm^{-1}); ν(N-H): 3191m; ν(C-H, arom.): 3098w, 3077w; ν(C=O): 1728s; ν(C=N): 1610s; ν(C=C): 1568s and 1556s; ν(N-O): 991w. ^{1}H NMR in *DMSO-d₆, δ* ppm: 2.32 (s, 3H), 7.43 (dd, *J* = 7.32, 1.22 Hz, 1H), 7.90 (dd, *J* = 7.32, 1.40 Hz, 1H), 8.13 (d, *J* = 8.49, 1H), 8.30 (d, *J* = 8.42, 1H), 13.86 (s, 1H). ^{13}C NMR in *DMSO-d₆, δ* ppm: 9.94, 116.88, 125.20, 126.00, 126.03, 135.35, 136.81, 136.59, 159.73, 162.35.

(Z)-4-(2-(3-chlorophenyl)hydrazono)-3-methylisoxazol-5(4H)-one (**15**): Crude yield: 95.5%. Final Yield: 89.7% MP: 161-162 ºC. Anal. Calc. (%) for $C_{10}H_8ClN_3O_2$ (Mɪ: 237,64 g/mol): C, 50.54; H, 3.39; N, 17.68; Found (%): C, 50.27; H, 4.46; N, 17.26. UV-visible spectrum in ethanol solution 2.5

View Article Online
DOI: 10.1039/C5NJ02604K

$\times 10^{-5}$ mol/L, λ_{max}, nm (log**ε**): 390(4.22); 260sh(3.91); 252(4.00); 202(4.28). I.R. spectrum in solid state, $\overline{\nu}$ (cm^{-1}); ν(N-H): 3207s; ν(C-H, arom.): 3132w, 3088w, 3068w, 3031w; ν(C-H, aliph.): 2928w; ν(C=O): 1716s; ν(C=N): 1586sh; ν(C=C): 1564s; ν(N-O): 991w. ^{1}H NMR in *CDCl*$_3$, *δ* ppm: 2.33 (s, 3H), 7.24-7.19 (m, 2H), 7.35 (t, *J* = 8.06 Hz, 1H), 7.48 (t, *J* = 2.00 Hz, 1H), 12.55 (s, 1H). ^{13}C NMR in *CDCl*$_3$, *δ* ppm: 10.22, 114.41, 115.95, 122.31, 126.51, 130.82, 135.94, 141.54, 159.32, 164.64.

Biological studies

Tissue Culture: The HL-60, promyelocytic leukemia cell line, was purchased from the American Type Culture Collection-ATCC (Manassas, VA). This cell line was collected from peripheral blood cells of a 36-year old Caucasian female with acute promyelocytic leukemia (APL) and they grow as a suspension culture. The predominant cell population consists of neutrophilic promyelocytes[26,27]. In the laboratory, these cells were stored under liquid nitrogen until use. Then, they were thawed by gentle stir of their containers (vials) during 2 minutes in a water bath at 37 ºC. After thawing, the content of each vial of cells was transferred into a 25 cm2 tissue culture flask, T-25, diluting with 10 mL of RPMI 1640 containing 1 mmol/L L-glutamine (GIBCO/BRL, Gaithersburg, MD), supplemented with 10% (v/v) of fetal bovine serum (FBS) and 1% (w/v) penicillin/streptomycin. The T-25 flask (2 x 10^6 viable cells) was observed under the microscope, followed by incubation in a humidified 5% CO2 at 37 °C. Three times a week, the culture cells was diluted under same conditions in order to maintain a density of 5 x 10^5 cells/mL and harvested in the exponential phase of growth. The cell viability was assessed by the Trypan Blue exclusion test (Life Technologies) and manually counted using a hemocytometer.

View Article Online
DOI: 10.1039/C5NJ02604K

Cytotoxicity/MTT Assay: This colorimetric assay measures the reduction of 3-(4,5-dimethylthiasol-2-yl)-2,4,-diphenyltetrazolium bromide (MTT) by mitochondrial succinate dehydrogenase. The MTT enters the cells and passes to the mitochondria where is reduced to formazan, an insoluble colored product. In order to dissolve the formazan, the cells are then treated with an organic solvent (DMSO or isopropanol) and the obtained solution is measured spectrophotometrically between 530-650 nm range[28,29].

Aliquots of 200 µL of HL-60 cell suspension (5x 105 cells/mL) were seeded into 96 well polystyrene tissue culture plates, an aliquot of 1.0 µL of isoxazolone (2.0, 5.0, 8.0, 12.0, 20.0, 30.0, 40.0, 60.0, 80.0 and 100.0 µM) and, carefully, were also added to each well using DMSO:EtOH (1:4) as solvent and vehicle control. Cells incubated in culture medium alone served as a control for cell viability (untreated wells). Cells were placed in the humidified 5% CO2 incubator at 37°C for 24 hours. After incubation, 10 µL aliquots of MTT solution (5 mg/mL in PBS) were added to each well and re-incubated for 4 hours at 37° C, followed by low centrifugation at 800 rpm for 5 minutes. Then, the 200 µL of supernatant culture medium were carefully aspirated and 200 µL aliquots of dimethylsulfoxide (DMSO) were added to each well in order to dissolve the formazan crystals, followed by incubation during 10 minutes. The culture plate was placed on an Emax model micro-plate reader (Molecular Devices) and the absorbance was measured using a 650 nm filter. The amount of color produced is directly proportional to the number of viable cells. All assays were performed four times with three replicates each one processed independently and means ± SD values were used to estimate the cell viability. Cell viability rate was calculated as the percentage of MTT absorption as follows:

$$\% \text{ survival} = (\text{mean experimental absorbance}/\text{mean control absorbance}) \times 100.$$

View Article Online
DOI: 10.1039/C5NJ02604K

The isoxazolone concentration was plotted against the corresponding percentage (%) of cell viability obtained with MTT assays, and the 50% inhibitory concentration (IC_{50}) was calculated by non-linear regression using fitting with Sigmaplot©11 program from Systat Software, Inc. As positive control Paclitaxel was used, see Figure S1.

Semiquantitive duplex RT-PCR: Total RNA was isolated from cells using Chomczynski's method[30] and quantified by measuring of its optical density at 260 nm. First strand cDNA was synthesized with 2 µg of total RNA in a buffer containing 100 pmol of oligo dT, dNTPs 0.25 mM, DTT 10 mM, 20U of RNase Inhibitor and 50U of M-MLV Reverse Transcriptase (Invitrogen). The mixture was incubated for 1 h at 42◦ C. The PCR amplifications were carried out using GoTaq Green Master Mix (Promega). For quantitative analysis of Bcl-2, $p21^{WAF-1}$, and Bax mRNAs, human glyceraldehyde-3-phosphate dehydrogenase (G3PDH) gene served as the internal control for calculation of the densitometry results. The primers were designed based on the sequences of the gene bank:

Bcl-2	(F), 5`-TGCACCTGACGCCCTTCAC-3`
	(R), 5`-AGACAGCCAGGAGAAATCAAACAG-3`
Bax	(F), 5`-ACCAAGAAGCTGAGCGAGTGTC-3`
	(R), 5`-ACAAAGATGGTCACGGTCTGCC-3`
$p21^{WAF-1}$	(F), 5`-GG-GGACAGCAGAGGAAGAC-3`
	(R), 5`-CGGCGTTTGGAGTGGTAGA-3`
GAPDH	(F), 5`-ACCCAGAAGACTGTGGATGG-3`
	(R), 5`-CCCCTCTTCA-AGGGGTCTAC-3`

View Article Online
DOI: 10.1039/C5NJ02604K

The PCR products were separated using 1.5% agarose gels. After the gels were stained with ethidium bromide, gel images were obtained and the densities of the products were quantified using Gel-Pro Analyzer 4.0 Software (Media Cybernetics, USA). All experiments were repeated at least four times. Figures showing the images of the electrophoresis of PCR products correspond to one of several repetitions of the three independent experiments performed, and were chosen because it clearly shows the bands under study; the images used for quantification do not necessarily correspond to those shown, because unsaturated images were chosen for proper quantification.

Statistical Analysis: Data were compared by one-way analysis of variance Student's t-test to determine statistical significance (Sigmaplot©11). Each experiment is performed in triplicate on 4 occasions. Results are expressed as mean ± SD. Differences with P values of < 0.05 were considered significant.

Computational Details. The Gaussian 09 computational package[31] was used to perform ground-state and transition-state geometry optimization calculations employing Becke's three-parameter hybrid exchange functional and the Lee−Yang−Parr nonlocal correlation functional B3LYP[32–34] and the 6-31G* basis set was used for C, N, O, Cl, Br, and H atoms[35]. The Hessian was computed of all investigated compounds in order to characterize them as minima and no imaginary values were found. Time-dependent DFT (TDDFT) calculations were also performed using this methodology, and the first 60 singlet excited states were calculated. Calculations by the first-principles method were used to obtain accurate excitation energies and oscillator strengths. We modelled the effect of the solvent with the polarizable continuum model (PCM) using ethanol as solvent[36] for the optimization and TDDFT calculations, see Figure S2 for all the FMO involved in the transitions.

View Article Online
DOI: 10.1039/C5NJ02604K

RESULTS AND DISCUSSION

Synthesis

Under inert atmosphere and prolonged reflux in ethanol the precursor compounds β-hydrazodiketone, R-$C_6H_4NHN=C(COCH_3)(COOCH_2CH_3)$ (R= *4*-OH (**1**), *4*-OCH_3 (**2**), *4*-CH_3 (**3**), *4*-H (**4**), *4*-Cl (**5**), *4*-Br (**6**) *4*-CO_2H (**7**), *4*-$COCH_3$ (**8**), *4*-CN (**9**), *4*-NO_2 (**10**), 2-OH (**11**), 2-Cl (**12**), 2-CO_2H (**13**), 2-NO_2 (**14**), 3-Cl (**15**)) reacts with hydroxylamine hydrochloride affording in good yield a series of yellow-orange oxazolones, **1-15**, see Scheme 1. The low yield observed for **1** might be explained due to the presence of the hydroxyl substituent group in *para* position which enhances the solubility of this compound. In concordance with the scheme, we propose that these reactions form an intermediate oxime that after a long time refluxed suffers a subsequent cyclization reaction yielding the corresponding product. The information contrasts with the literature, where it becomes established that the hefts of reactions require strong bases, strong mineral acids, high temperatures[14–16]. Contrarily, the reactions presented here occur in one step, under mild conditions of reflux in ethanol during 18 H, catalyzed by a weak organic acid, HOAc, and with high regioselectivity. The purification was performed in every case via a recrystallization from hot ethanol. All the synthetized compounds were characterized using elemental analysis and spectroscopic techniques *vide infra*. Additionally, suitable crystals for X-Ray diffraction were obtained and it was possible to resolve the structure of **4**, **12**, **15**. Compound **4** was previously reported[25] and our structure is in concordance with this previous report, whereas the crystallization in this case was performed allowing the solution to slowly evaporate the ethanol.

View Article Online
DOI: 10.1039/C5NJ02604K

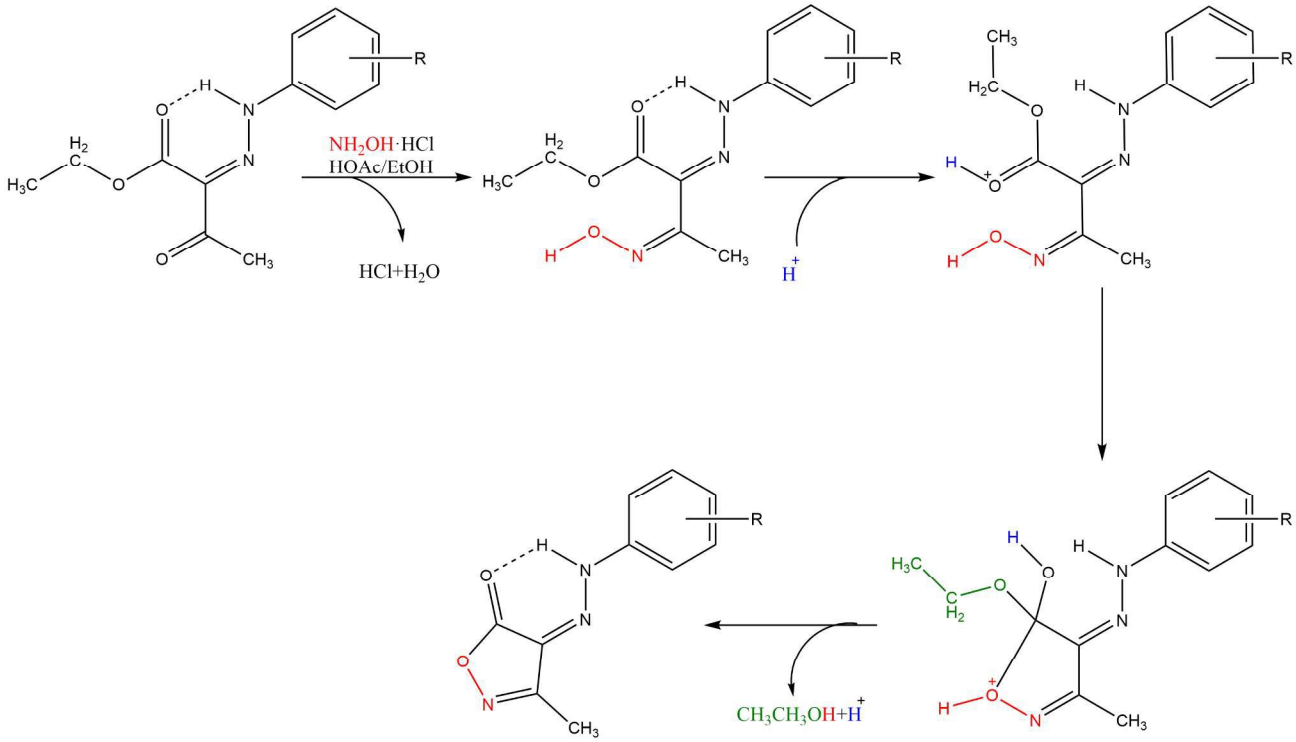

R= 4-OH (**1**); 4-CH_3 (**2**); 4-OCH_3 (**3**); 4-H (**4**); 4-Cl (**5**); 4-Br (**6**); 4-CO_2H (**7**); 4-$COCH_3$ (**8**); 4-CN (**9**); 4-NO_2 (**10**); 2-OH (**11**); 2-Cl (**12**); 2-CO_2H (**13**); 2-NO_2 (**14**); 3-Cl (**15**)

Scheme 1. Proposed reaction mechanism.

Structure description

For compounds **4**, **12** and **15** suitable crystals were obtained for X-Ray diffraction (as shown in Figure 2). Those compounds showed C2/c, $P\bar{1}$, P2(1)/c spatial groups, respectively. The unitary cell of the compounds showed Z=8, Z=2 and Z=8, respectively. An ORTEP diagram for each compound can be found in Figure 2. Surprisingly, compound **15** showed 4 pairs of isoxazolone molecules slightly different, which are labeled as **15a** and **15b**. Table S1 showed the most important distances and angles for these molecules. In the theoretical section a comparison between these experimental distances and the calculated distances will be made. The observed distances for the studied compounds are in good agreement with similar reported molecules[37–39]. For further details please see the SI. All the molecules showed almost a planar structure, with a dihedral angle smaller than 3°.

View Article Online
DOI: 10.1039/C5NJ02604K

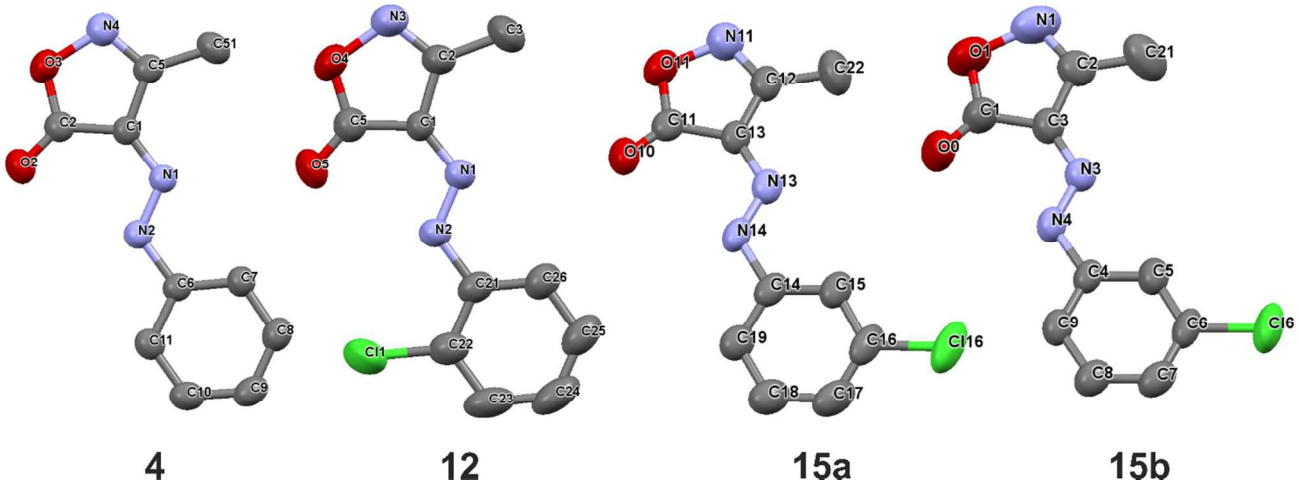

Figure 2. ORTEP diagram with a 50% of probability for compounds **4**, **12** and **15**.

Spectroscopic studies

The UV-visible spectra of compounds **1-15**, see Table 2, registered in ethanol solutions exhibit two principal absorption bands in the range 427-222 nm. We believe that the first observed band, λ_1, located in 427-390 nm range, is associated with a $\pi^* \leftarrow \pi$ transition due to the conjugated aromatic heterocyclic system. The second observed band, λ_2, placed in 343-254 nm range, probably, is due to $\pi^* \leftarrow \pi$ transition centered in the chromophore -N-N-. Other high energy absorption bands, located around 250 nm and lower, may be due to internal transition in the aromatic rings. The expected behaviour for the first three calculated transitions was corroborated via theoretical calculations, *vide infra*.

Table 2. UV-visible absorption bands (in nm) of **1-15** in ethanol solution, calculated extinction coefficient (log**ε**) in parentheses and their corresponding Hammett parameters (σ).

View Article Online
DOI: 10.1039/C5NJ02604K

Comp.	σ	λ_1	λ_2	λ_3	λ_4	λ_5
1	-0.37	427(4.40)	300(3.43)	252(4.00)	---	---
2	-0.27	421(4.42)	303(3.42)	252(4.02)	237h(4.02)	---
3	-0.17	405(4.37)	260h(3.94)	253(4.02)	---	---
4	0	396(4.40)	255(3.99)	249(4.05)	---	---
5	0.23	397(4.42)	258h(3.95)	250(4.05)	238h(3.96)	---
6	0.23	399(4.45)	260h(3.97)	251(4.06)	237h(3.97)	---
7	0.45	396(4.50)	265h(4.04)	256(4.07)	---	---
8	0.5	399(4.36)	276(3.89)	254(3.89)	246(3.79)	222(3.94)
9	0.66	391(4.50)	254(4.09)	---	---	---
10	0.78	400(4.59)	297(3.73)	---	---	---
11		425(4.37)	259h(3.78)	245(3.91)	---	---
12		395(4.17)	260(3.70)	252(3.80)	246h(3.79)	---
13		399(4.41)	273h(3.86)	264(3.97)	227(4.07)	---
14		410(4.32)	343(4.09)	281(3.99)	248h(4.10)	---
15		390(4.32)	259h(3.91)	252(3.99)	---	---

A Hammett correlation plot was performed for all the observed UV-Vis transitions, but no correlation was observed (data not shown). Nevertheless, a trend is observed for the transitions, where λ_1 and λ_2 show a bathochromic shift which might be due to the effect that has the R group over the azo ring.

The infrared spectra of **1-15** could be found in the SI. These spectra on KBr disc exhibit the typical aromatic and aliphatic ν(C-H) absorptions bands, around 3000 cm^{-1}, respectively. On the other hand, at least three intense absorption bands emerge in the range 1611-1495 cm^{-1}. Those signals are typical

View Article Online
DOI: 10.1039/C5NJ02604K

for the ν(C=N) and ν(C=C) chromophores presents on the oxazolone and aromatic rings. The substituent groups, R, of compound **7**, **8** and **13** show the characteristic carbonyl stretching mode, ν(C=O), at 1673, 1678 and 1676 cm^{-1}, respectively. The ν(N-O) stretching mode of the oxazolone ring may be found closely around 1250 cm^{-1}. The most remarkable signal correspond to the ν(N-H) signal that can be observed in almost all the compound located between 3188-3212 cm^{-1}, however in case of compounds **1**, **11** and **13** this band is not observed due to the presence of the intense ν(O-H) band at the same frequency. In case of compound **4** despite the presence of the intense ν(O-H) signal, the ν(N-H) was observed at higher frequency. This spectral information is in concordance with those given previously in literature[40].

Tables 3 and S3 shows the chemical shift and the assignment of each signals observed in the ^{1}H-NMR and ^{13}C-NMR spectra of compounds **1-15**, respectively. Both series of spectra were recorded in $CDCl_3$ or DMSO-d_6 solutions and all the signals were successfully assigned with help of the HMBC spectra. Figure 3 exhibits a typical HMBC spectrum obtained for **3**. For compound **13** the signals for N-H and 2-COOH were not clearly observed, however they are attributed as a broad signal between 2.50-7.00 ppm. For the rest of the compounds all the expected signals were observed. The first signal attributed to the -CH_3 group, located between 2.35-2.23 ppm. The aromatic signals were observed between 6.66-8.07 ppm. In case of the N-H signal it was observed for all compounds over 11.16 ppm. Furthermore, the signal expected for the substituent over the azo benzene ring was also observed at different locations, depending on the character of the substituent, see Table 3. The integrals for all the mentioned signals are in concordance with the number of expected protons. In case of the ^{13}C-NMR signals, it was possible to do the assignation of all the expected signals for all the synthetized compounds. The most relevant finding in this sense is the location of the carbons located in the oxazolone ring, which are common to all the studied compounds for C_1, C_2, C_3 and C_4, see Table S2. The conjugation of the fragment -N=C-C=N-NH-

View Article Online
DOI: 10.1039/C5NJ02604K

that binds the azophenyl substituted ring is interrupted in the -NH-Ar. This situation prevents any important influence in any measured spectroscopical property.

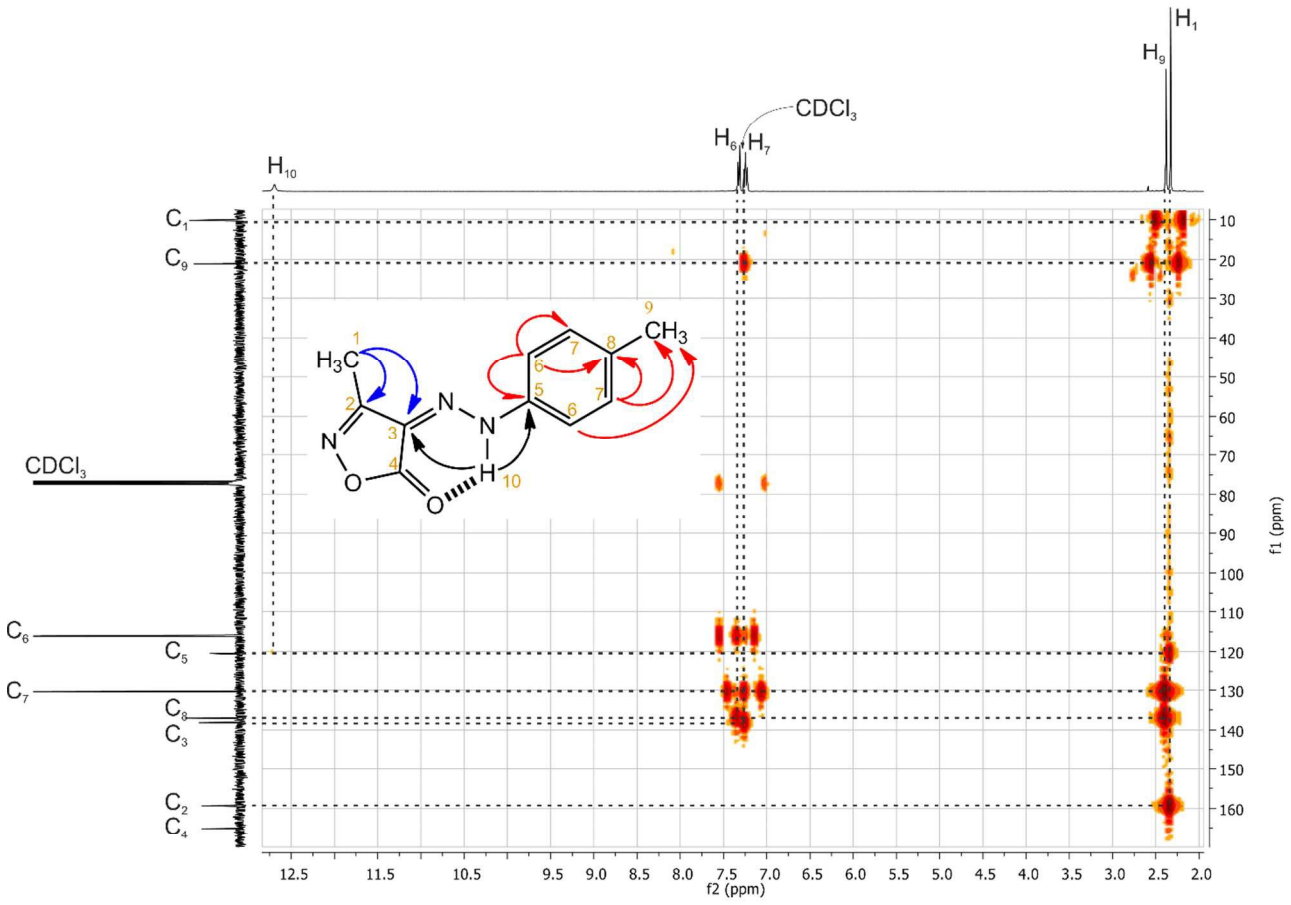

Figure 3. HMBC spectrum of compound **3** in $CDCl_3$ showing the H-C interactions.

Table 3. Chemical shift signals (δ: ppm) in the ^{1}H-NMR spectra of **1-15** in $CDCl_3$.

View Article Online
DOI: 10.1039/C5NJ02604K

	CH_3	H(Ar)	N-H	H(R)
1	2.23 (s, 3H)	7.69 – 7.38 (m, 2H) 6.95 – 6.66 (m, 2H)	12.80 (s, 1H)	9.76 (s, 1H)
2	2.32 (s, 3H)	7.40 – 7.35 (m, 2H) 6.99 – 6.94 (m, 2H)	12.78 (s, 1H)	3.84 (s, 3H)
3	2.32 (s, 3H)	7.32 (d, J = 8.5 Hz, 2H) 7.23 (d, J = 8.4 Hz, 2H)	12.69 (s, 1H)	2.38 (s, 3H)
4	2.34 (s, 3H)	7.47 – 7.40 (m, 4H)) 7.28 (m, 1H)	12.67 (s, 1H)	---
5	2.33 (s, 3H)	7.43 – 7.39 (m, 2H) 7.38 – 7.34 (m, 2H)	12.64 (s, 1H)	---
6	2.33 (s, 3H)	7.64 – 7.47 (m, 2H) 7.34 – 7.28 (m, 2H)	12.65 (s,1H)	---
7	2.26 (s, 3H)	8.02 – 7.96 (m, 2H) 7.78 – 7.72 (m, 2H)	12.78 (s, 1H)	12.93 (s, 1H),
8	2.35 (s, 3H)	8.07 – 8.02 (m, 2H) 7.50 – 7.46 (m, 2H)	12.64 (s, 1H)	2.61 (s, 3H)
9	2.35 (s, 3H)	7.73 (d, J = 8.8 Hz, 2H) 7.51 (d, J = 8.8 Hz, 2H)	12.58 (s, 1H),	---
10	2.27 (s, 3H)	8.34 – 8.26 (m, 1H) 7.91 – 7.83 (m, 1H)	11.16 (s, 1H),	---
11	2.26 (s, 3H)	7.60 (dd, J = 8.1, 1.5 Hz 1H) 7.15 – 7.08 (m, 1H) 7.01 – 6.91 (m, 2H)	12.75 (s, 1H)	10.79 (s, 1H),
12	2.34 (s, 3H)	7.78 (dd, J = 8.3, 1.2 Hz, 1H) 7.43 (dd, J = 8.0, 1.2 Hz, 1H) 7.40 – 7.33 (m, 1H)	12.94 (s, 1H)	---
13	2.26 (s, 3H)	7.18 (td, J = 8.0, 1.5 Hz, 1H) 7.99 (dd, J = 7.9, 1.3 Hz, 1H) 7.92 (d, J = 8.2 Hz, 1H) 7.74 – 7.66 (m, 1H) 7.38 – 7.22 (m, 1H)	No Obs.	No Obs.
14	2.32 (s, 3H)	8.29 (d, J = 8.4 Hz, 1H) 8.12 (d, J = 8.4 Hz, 1H) 7.90 (t, J = 7.9 Hz, 1H) 7.43 (t, J = 7.8 Hz, 1H) 7.49 (t, J = 2.0 Hz, 1H)	13.85 (s, 1H)	---
15	2.34 (s, 1H)	7.36 (td J = 8.0, 5.2 Hz, 1H) 7.23 (dddd, J = 10.6, 8.0, 2.0, 0.8 Hz, 2H)	12.56 (s, 1H),	---

View Article Online
DOI: 10.1039/C5NJ02604K

Theoretical calculations

In order to perform a better description of the studied compounds DFT and TDDFT calculations were performed for all the synthetized compounds. All the calculated geometrical parameters show a good agreement with the obtained X-Ray diffraction distances, see Table 4. When all the studied compounds are compared, it can be observed that the calculated bond distances remain almost unaltered as the substituent is changed over the azophenyl ring. Furthermore all the molecules show a planar structure.

Table 4. Table 4. Selected bond distances for compounds **1-15** in Angstroms, compared with the corresponding distances of the X-Ray diffraction in brackets and the XRD values of each measurement in parentheses.

Comp.	C-R	C6-N2	N2-N1	N1-C1	<N1N2HO2	O3-N4
1	1.368	1.407	1.308	1.317	0	1.449
2	1.51	1.406	1.309	1.315	0	1.449
3	1.364	1.407	1.307	1.317	0	1.449
4	1.085 [0.930]	1.406 [1.420(2)]	1.310 [1.313(2)]	1.314 [1.315(2)]	0 [4.12]	1.449 [1.475(3)]
5	1.755	1.404	1.311	1.313	0	1.45
6	1.901	1.403	1.311	1.313	0	1.45
7	1.484	1.401	1.314	1.31	0	1.45
8	1.498	1.401	1.314	1.311	0	1.45
9	1.433	1.4	1.316	1.309	0	1.45
10	1.467	1.398	1.317	1.308	0	1.451
11	1.37	1.403	1.311	1.313	0	1.448
12	1.751 [1.732(3)]	1.404 [1.395(3)]	1.312 [1.307(2)]	1.313 [1.296(3)]	0 [4.22]	1.452 [1.470(3)]
13	1.54	1.406	1.31	1.314	0	1.449
14	1.474	1.399	1.317	1.306	-3.6	1.454
15	1.756 [1.738(4)*]	1.404 [1.414(4)*]	1.312 [1.307(3)*]	1.312 [1.305(5)*]	0 [3.65*]	1.45 [1.537(4)*]

*Mean measured distance.

The isosurface of the frontier molecular orbitals were plotted for all the studied compounds, see Figure S1 in the SI. As can be observed the localization of those orbitals remains unaltered as the

View Article Online
DOI: 10.1039/C5NJ02604K

substituent is changed in the azophenyl ring from electron-donating to electron-withdrawing substituent. The HOMO is in all cases mainly localized over the two rings (oxazolone and azophenyl ring). On the other hand the LUMO is mainly localized over the oxazolone ring and over the =N-NH- bridge. The HOMO-LUMO gap (HLG) does not vary dramatically between the studied compounds, as might be expected due to the similarity observed in the UV-Vis spectra, *vide supra*. In this sense the HLG has a value of around 3.3eV for all the studied compounds.

In order to perform a better characterization of the UV-Vis spectra, TDDFT calculations were performed, see Table S3 in the SI. As can be observed, in all the studied compounds three main absorption bands are observed. In the TDDFT calculations the same number of transitions was observed. The first calculated transition corresponds in every case to a HOMO-LUMO transition ($\pi^* \leftarrow \pi$). Almost every second calculated transition goes from an occupied orbital to the LUMO+1 ($\pi^* \leftarrow \pi$). The third calculated transition does not show any trend. As observed in the first and second transition a small dependency on the change of the substituent over the azophenyl ring is observed, which explains the small variation between the observed UV-Vis absorption profiles.

To make the first approach of the reactivity that this compounds might show, the estimated reactivity indexes (electronic chemical potential (μ), chemical hardness (η) and electrophilicity (ω))[41–43] are reported in Table 5. In all cases no clear tendency on the variation of the global index of reactivity was observed. η is a measure of the resistance of a chemical species to change its electronic configuration. It is thought as an indicator, together with electronegativity, of the chemical reactivity and stability of systems. The highest value for η is shown by **14**, which has the *o*-nitro substituent, which is the most electron-withdrawing substituent. On the other hand, the smallest value is shown by **1** which has the most electron-donating substituent. μ characterizes the tendency of escaping of electrons from the equilibrium system; it is then related to the electronic charge rearrangement

View Article Online
DOI: 10.1039/C5NJ02604K

associated to any chemical process. The lowest μ is shown by **14**, which has the most electron donor substituent, and the highest μ is shown by **3**.

Table 5. HOMO and LUMO energies, HLG and reactivity indexes, electronic chemical potential (μ), chemical hardness (η) and electrophilicity (ω), all in eV.

Comp.	HOMO	LUMO	HLG	μ	η	ω
1	-6.18	-2.89	3.29	-4.54	1.65	6.25
2	-6.33	-2.82	3.51	-4.58	1.76	5.96
3	-6.07	-2.86	3.21	-4.47	1.61	6.21
4	-6.5	-3.01	3.49	-4.76	1.75	6.48
5	-6.57	-3.16	3.41	-4.87	1.71	6.94
6	-6.54	-3.17	3.37	-4.86	1.69	6.99
7	-6.8	-3.34	3.46	-5.07	1.73	7.43
8	-6.75	-3.33	3.42	-5.04	1.71	7.43
9	-6.95	-3.49	3.46	-5.22	1.73	7.88
10	-7.13	-3.7	3.43	-5.42	1.72	8.55
11	-6.27	-2.88	3.39	-4.58	1.7	6.17
12	-6.6	-3.03	3.57	-4.82	1.79	6.49
13	-6.54	-3.05	3.49	-4.8	1.75	6.59
14	-6.98	-3.37	3.61	-5.18	1.81	7.42
15	-6.7	-3.18	3.52	-4.94	1.76	6.93

Electrophilicity index, ω, could give information comparing two molecules in which one is an electrophile (or nucleophile) and this is indicated by a higher (or lower) ω. In this case the highest value of ω was found for compound **10**, which has in position *para* a nitro group which is the most electron-withdrawing substituent. On the other hand the smallest value of ω was found for compound **2**.

Biological essays

Compounds **1** to **15** were subjected to *in vitro* biological studies by incorporating them to cultures of leukemia HL-60 cells. The cytotoxic effect was measured after exposure of the cells to the

View Article Online
DOI: 10.1039/C5NJ02604K

isoxazolones for 24 h, and this effect was expressed as the relative change on the cell viability compared to the control samples (untreated and vehicle treated cells). The IC_{50} values were obtained from dose-response curves and they fall in a wide range of concentrations, see Table 6. The isoxazolones **5**, **10**, **11** and **15** were the most active, with IC_{50} values between 73 and 83 μM. Each of four compounds mentioned, which showed the highest cytotoxic activity toward HL-60 cells, were subject of additional biological studies.

Table 6. Cytotoxic activity of the isoxazolones (IC_{50} values) on HL-60 cells and Standard Deviation in parenthesis.

	IC_{50} (μM)
1	111 (14)
2	606 (88)
3	283 (76)
4	160 (32)
5	81 (10)
6	167 (42)
7	142 (21)
8	ND (ND)
9	124 (42)
10	73 (7)
11	83 (24)
12	168 (37)
13	414 (41)
14	ND (ND)
15	77 (6)

*ND: Not Determined.

Effect of the isoxazolones on the expression of Bcl-2, Bax and $p21^{WAF-1}$**.** We also explored the effect of isoxazolones **5**, **10**, **11** and **15** on the expression genes involved in apoptosis and cell cycle progression. Apoptosis is an active process, named also programmed cell death, which occur in cells

View Article Online
DOI: 10.1039/C5NJ02604K

of multicellular organism in response to a variety of agents including heat, radiation, nutrient deprivation, viral infection, hypoxia, increased intracellular calcium concentration, or chemical exposition (including anticancer drugs)[44]. This implicates, inter alia, the balanced transcriptional control of anti-apoptotic and pro-apoptotic genes, such as Bax and Bcl-2. Within the antiproliferative mechanisms is also important to check the expression levels of $p21^{WAF-1}$, a genic product associated with the inhibition of the proliferation by cell cycle arrest; which we have also included in this study[45–47]. The protein $p21^{WAF-1}$ is a potent inhibitor of cyclin-dependent kinases (CDKs), in general also named cyclin-dependent kinase inhibitor (CKI) and can inhibit the phosphorylation of tumor suppressor proteins such as retinoblastoma protein (Rb); allowing these last exercise its oversight role on cell proliferation[48,49]. Thus, a stimulus that increase the expression of $p21^{WAF-1}$ signalize toward the cell cycle arrest and is therefore antiproliferative.

In order to determine the effect of isoxazolones **5**, **10**, **11** and **15** on Bax, Bcl-2 and $p21^{WAF-1}$ mRNA expression level, we performed a semi-quantitative duplex RT-PCR. Treatment of HL-60 cells during 24 h with compounds **5** and **10** at a concentration similar to its IC_{50} values respective, 80 and 70 μM, induced an important decrease on the expression of Bcl-2 to around 47% (Figures 4-A, lane 3; and Figures 4 D, **5**) and 43% (Figures 4 A, lane 4; and Figures 4 D, **10**) relative to the control ($P< 0.05$), respectively. Meanwhile, treatment with compounds **11** and **15** at concentrations of 80 and 75 μM during 24 h, increased the expression of Bcl-2 to 309% (Figures 4 A, lane 5; and Figures 4 D, **10**) and 207% (Figures 4 A, lane 6; and Figures 4 D, **15**) relative to the control ($P< 0.05$), respectively. Meanwhile, compounds **5**, **10** and **15** elicited no statistically significant increases to 164, 124 and 119% on Bax mRNA levels, respectively (Figures 4 B, lanes 3, 4, and 6; and Figures 4 E, **5**, **10** and **15**). Conversely, isoxazolone **11** induced a decrease to 54% of Bax mRNA levels (Figures 4 B, lane 5; and Figures 4 E, **11**) relative to the control ($P< 0.05$). On the other hand, we

View Article Online
DOI: 10.1039/C5NJ02604K

found that isoxazolones **5**, **10**, **11** and **15** elicited no statistically significant decrease of the levels of p21^{WAF-1} mRNA expression to 58, 81, 79 and 74% relative to the control, respectively (Figures 4 C, lanes 3-6; and Figures 4 F, **5**, **10**, **11** and **15**).

These results suggest that the cytotoxic activity of the isoxazolones **5** and **10** would be the sum of positive modulation on signals to promotion of apoptosis and negative modulation on anti-apoptotic mechanisms, without a clear consequence on cell cycle. While, the cytotoxic effect observed for isoxazolones **11** and **15** seems to be through mechanisms other than those analyzed in this work. Furthermore, for this family of compounds, it is observed that the electrophilicity index values calculated by means of DFT get smaller while the biological activity gets bigger, which might correlate the observed activity against cancer cell lines and the calculated reactivity indexes.

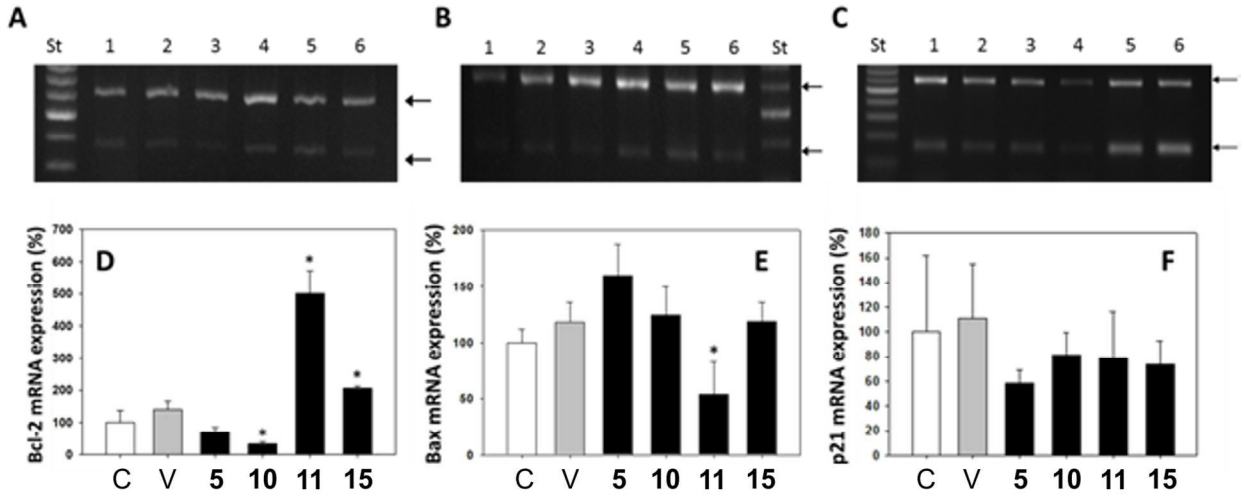

Figure 4. Effect of the isoxazolones 5, 10, 11 and 15 on mRNA expression levels of Bcl-2 (A and D), Bax (B and E) and p21^{WAF-1} (C and F) in HL-60 cells examined by semiquantitive duplex RT-PCR. PCR products were separated using 1.5% agarose gel electrophoresis, the arrows indicate the PCR products for GAPDH (600 bp, upper arrow in all cases), Bcl-2 (293 bp), Bax (332 bp) and p21^{WAF-1} (156 bp). Lane 1, untreated control (C); line 2, vehicle control (V); lane 3, treatment with

View Article Online
DOI: 10.1039/C5NJ02604K

80 μM isoxazolone **5**; lane 4, 70 μM isoxazolone **10**; line 5, 80 μM isoxazolone **11**; and line 6, 75 μM isoxazolone **15**. The PCR products were quantified relative to the internal standard GAPDH (D, E and F). The results are shown as mean ± standard deviations (SD) and correspond to the percentage change compared to the control sample assigned as 100%. Differences with P values of < 0.05 (*) were considered significant.

CONCLUSIONS

The one-pot synthesis of a family of 3,4,5-trisubstituted isoxazolones has been carried out with good yields, by treatment of β-diketohydrazones of the type ethyl-2-(2-(*R*-phenyl)hydrazinylidene)-3-oxobutanoates with hydroxylammonium chloride in ethanol and acetic acid as a catalyst. All compounds were characterized using elemental analysis and spectroscopic methods. The crystalline and molecular structure of **4**, **12** and **15** has been determined by X-ray diffraction methods. The analytical, spectroscopic and structural data are in concordance with the proposed structures and with the data obtained from literature[25].

The UV-Visible spectra showed three to four absorption bands, which were not affected by the nature of the substituent located around the azophenyl substituted ring, showing that the electronic communication is truncated due to the presence of the =N-NH- bridge. A similar behaviour was observed for the other spectroscopical measurements. Furthermore density functional theory and time dependent density functional theory calculations were performed in order to give a better explanation to the observed UV-Vis bands. As shown by the calculations the geometries of the compounds and the time dependent density functional theory calculated transitions, there is no variation in both measured properties as the substituent located around the azophenyl substituted ring is changed due to the constant composition of the involved molecular orbitals.

View Article Online
DOI: 10.1039/C5NJ02604K

Finally, the cytotoxic activity of these compounds was evaluated on human promyelocytic leukemia cells, HL-60. Isoxazolones **5**, **10**, **11** and **15** exhibit a significant cytotoxic activity, with IC_{50} values below 83 μM and thus they emerge as potential molecules for further antineoplasic studies. In this context, the effect of these compounds on the expression of genes involved in apoptosis and in the cell cycle control has been evaluated. Compounds **5** and **10** induce positively signals pro-apoptotic, and negatively signal anti-apoptotic, since the level of Bcl-2 mRNA decreases to approximately 45% in both cases, and Bax mRNA increase to 160 and 124%, respectively. On the other hand, the cytotoxic effect observed for isoxazolones **11** and **15** seems to be independent of the mechanisms analyzed in this work.

Acknowledgements. The authors greatly acknowledge the financial support received from Dirección de Investigación y Desarrollo, DID-UACh, of the Universidad Austral de Chile, Grant Nº S 2003-03 and also to FONDECYT 1120903 and 1130707.

Supporting Information. In the supporting information might be found the CIF file for compound **4**, Figure S1 with the Paclitaxel positive control graph, Table S1 with the selected bond lengths, Table S2 with a summary of the ^{13}C-NMR signals, Table S3 with the information of the TD-DFT calculations, Figure S2 with the FMOs for all the compounds, The full UV-Vis, ^{1}H-NMR, ^{13}C-NMR and HBMC spectra for all the compounds.

REFERENCES

1. T. Kietzke, *Adv. Optoelectron.*, 2007, **2007**.

2. M. Rowley, H. B. Broughton, I. Collins, R. Baker, F. Emms, R. Marwood, S. Patel, S. Patel, C. I. Ragan, S. B. Freedman, and P. D. Leeson, *J. Med. Chem.*, 1996, **39**, 1943–1945.

3. B. Frølund, A. T. Jørgensen, L. Tagmose, T. B. Stensbøl, H. T. Vestergaard, C. Engblom, U. Kristiansen, C. Sanchez, P. Krogsgaard-Larsen, and T. Liljefors, *J. Med. Chem.*, 2002, **45**, 2454–2468.

View Article Online
DOI: 10.1039/C5NJ02604K

4. G. Daidone, D. Raffa, B. Maggio, F. Plescia, V. M. C. Cutuli, N. G. Mangano, and A. Caruso, *Arch. Pharm. (Weinheim).*, 1999, **332**, 50–54.

5. A. H. Bhatt, H. H. Parekh, and A. R. Parikh, *Heterocycl. Commun.*, 1998, **4**, 361–366.

6. J. J. Talley, D. L. Brown, J. S. Carter, M. J. Graneto, C. M. Koboldt, J. L. Masferrer, W. E. Perkins, R. S. Rogers, A. F. Shaffer, Y. Y. Zhang, B. S. Zweifel, and K. Seibert, *J. Med. Chem.*, 2000, **43**, 775–777.

7. J. J. Talley, in *Progress in Medicinal Chemistry*, 1999, vol. 36, pp. 201–234.

8. M. P. Giovannoni, C. Vergelli, C. Ghelardini, N. Galeotti, A. Bartolini, and V. Dal Piaz, *J. Med. Chem.*, 2003, **46**, 1055–1059.

9. W. T. Li, D. R. Hwang, C. P. Chen, C. W. Shen, C. L. Huang, T. W. Chen, C. H. Lin, Y. L. Chang, Y. Y. Chang, Y. K. Lo, H. Y. Tseng, C. C. Lin, J. S. Song, H. C. Chen, S. J. Chen, S. H. Wu, and C. T. Chen, *J. Med. Chem.*, 2003, **46**, 1706–1715.

10. T. Bandiera, P. Grünanger, and F. M. Albini, *J. Heterocycl. Chem.*, 1992, **29**, 1423–1428.

11. P. Cuadrado, A. M. Gonzalez-Nogal, and R. Valero, *Tetrahedron*, 2002, **58**, 4975–4980.

12. C. B. Vicentini, A. C. Veronese, T. Poli, M. Guarneri, P. Giori, and V. Ferretti, *J. Heterocycl. Chem.*, 1990, **27**, 1481–1484.

13. Y. He and N.-H. Lin, *Synthesis (Stuttg).*, 1994, **1994**, 989–992.

14. G. N. Barber and R. A. Olofson, *J. Org. Chem.*, 1978, **43**, 3015–3021.

15. T. J. Nitz, D. L. Volkots, D. J. Aldous, and R. C. Oglesby, *J. Med. Chem.*, 1994, **59**, 5828–5832.

16. S. E. Denmark and J. M. Kallemeyn, *J. Org. Chem.*, 2005, **70**, 2839–2842.

17. R. A. Day, J. A. Blake, and C. E. Stephens, *Synthesis (Stuttg).*, 2003, **2003**, 1586–1590.

18. E. Bey, S. Marchais-Oberwinkler, P. Kruchten, M. Frotscher, R. Werth, A. Oster, O. Algül, A. Neugebauer, and R. W. Hartmann, *Bioorganic Med. Chem.*, 2008, **16**, 6423–6435.

19. E. Garattini, E. Parrella, L. Diomede, M. Gianni', Y. Kalac, L. Merlini, D. Simoni, R. Zanier, F. F. Ferrara, I. Chiarucci, P. Carminati, M. Terao, and C. Pisano, *Blood*, 2004, **103**, 194–207.

20. J. Kaffy, R. Pontikis, D. Carrez, A. Croisy, C. Monneret, and J.-C. Florent, *Bioorg. Med. Chem.*, 2006, **14**, 4067–4077.

21. D. Simoni, R. Rondanin, R. Baruchello, M. Rizzi, G. Grisolia, M. Eleopra, S. Grimaudo, A. Di Cristina, M. R. Pipitone, M. R. Bongiorno, M. Aricò, F. P. Invidiata, and M. Tolomeo, *J. Med. Chem.*, 2008, **51**, 4796–4803.

22. C.-M. Sun, L.-G. Lin, H.-J. Yu, C.-Y. Cheng, Y.-C. Tsai, C.-W. Chu, Y.-H. Din, Y.-P. Chau, and M.-J. Don, *Bioorg. Med. Chem. Lett.*, 2007, **17**, 1078–1081.

23. H. C. Yao and P. Resnick, *J. Am. Chem. Soc.*, 1962, **84**, 3514–3517.

24. G. M. Sheldrick, *Acta Crystallogr. Sect. A Found. Crystallogr.*, 1990, **46**, 467–473.

25. V. Bertolasi, P. Gilli, V. Ferretti, and G. Gilli, *Acta Crystallogr. Sect. B Struct. Sci.*, 1994, **50**, 617–625.

26. R. I. Freshney, *Culture of Animal Cells: A Manual of Basic Technique*, 5th edn., 2005.

View Article Online
DOI: 10.1039/C5NJ02604K

27. J. Paul, *Culture, Cell and Tissue*, Churchill Livingstone, 5th edn., 1975.

28. P. B. Tchounwou, B. Wilson, J. Schneider, and A. Ishaque, *Met. Ions Biol. Med.*, 2000, **6**, 89–91.

29. T. Mosmann, *J. Immunol. Methods*, 1983, **65**, 55–63.

30. P. Chomczynski and N. Sacchi, *Anal. Biochem.*, 1987, **162**, 156–159.

31. Gaussian 09, Revision B.01, M. J. Frisch, G. W. Trucks, H. B. Schlegel, G. E. Scuseria, M. A. Robb, J. R. Cheeseman, G. Scalmani, V. Barone, B. Mennucci, G. A. Petersson, H. Nakatsuji, M. Caricato, X. Li, H. P. Hratchian, A. F. Izmaylov, J. Bloino, G. Zheng, J. L. Sonnenberg, M. Hada, M. Ehara, K. Toyota, R. Fukuda, J. Hasegawa, M. Ishida, T. Nakajima, Y. Honda, O. Kitao, H. Nakai, T. Vreven, J. A. Montgomery, Jr., J. E. Peralta, F. Ogliaro, M. Bearpark, J. J. Heyd, E. Brothers, K. N. Kudin, V. N. Staroverov, R. Kobayashi, J. Normand, K. Raghavachari, A. Rendell, J. C. Burant, S. S. Iyengar, J. Tomasi, M. Cossi, N. Rega, J. M. Millam, M. Klene, J. E. Knox, J. B. Cross, V. Bakken, C. Adamo, J. Jaramillo, R. Gomperts, R. E. Stratmann, O. Yazyev, A. J. Austin, R. Cammi, C. Pomelli, J. W. Ochterski, R. L. Martin, K. Morokuma, V. G. Zakrzewski, G. A. Voth, P. Salvador, J. J. Dannenberg, S. Dapprich, A. D. Daniels, Ö. Farkas, J. B. Foresman, J. V. Ortiz, J. Cioslowski, and D. J. Fox, Gaussian, Inc., Wallingford CT, 2009, .

32. A. D. Becke, *Phys. Rev. A*, 1988, **38**, 3098–3100.

33. C. Lee, W. Yang, and R. G. Parr, *Phys. Rev. B*, 1988, **37**, 785–789.

34. A. D. Becke, *J. Chem. Phys.*, 1993, **98**, 5648–5652.

35. P. J. Hay and W. R. Wadt, *J. Chem. Phys.*, 1985, **82**, 270.

36. M. Cossi, G. Scalmani, N. Rega, and V. Barone, *J. Chem. Phys.*, 2002, **117**, 43.

37. D. a. Mac-Leod-Carey, C. Bustos, E. Schott, L. Alvarez-Thon, and M. Fuentealba, *Acta Crystallogr. Sect. E Struct. Reports Online*, 2007, **63**, m670–m672.

38. C. Bustos, M. Pérez-Cerda, L. Alvarez-Thon, E. Barrales-Salcedo, and M. T. Garland, *Acta Crystallogr. Sect. E Struct. Reports Online*, 2012, **E68**, o353–o354.

39. C. Bustos, C. Sánchez, E. Schott, L. Alvarez-Thon, and M. Fuentealba, *Acta Crystallogr. Sect. E Struct. Reports Online*, 2007, **63**, o1138–o1139.

40. R. Faundez-Gutierreza, D. Macleod-Carey, X. Zarate, C. Bustos, E. Molins, E. Schott, *Polyhedron*, **81**, 2014, 414-420.

41. R. G. Pearson, *J. Mol. Struct. THEOCHEM*, 1992, **255**, 261–270.

42. R. G. Parr, L. Szentpaly, and S. Liu, *J. Am. Chem. Soc.*, 1999, **121**, 1922–1924.

43. P. K. Chattaraj and S. Giri, *Annu. Rep. Prog. Chem.{,} Sect. C Phys. Chem.*, 2009, **105**, 13–39.

44. D. E. Fisher, *Cell*, 1994, **78**, 539–542.

45. C. J. Sherr, *Cell*, 1993, **73**, 1059–1065.

46. T. Hunter, *Cell*, 1993, **75**, 839–841.

47. J. Kato, H. Matsushime, S. W. Hiebert, M. E. Ewen, and C. J. Sherr, *Genes Dev.*, 1993, **7**, 331–342.

View Article Online
DOI: 10.1039/C5NJ02604K

48. Y. Xiong, G. J. Hannon, H. Zhang, D. Casso, R. Kobayashi, and D. Beach, *Nature*, 1993, **366**, 701–704.

49. W. S. El-Deiry, T. Tokino, V. E. Velculescu, D. B. Levy, R. Parsons, J. M. Trent, D. Lin, W. E. Mercer, K. W. Kinzler, and B. Vogelstein, *Cell*, 1993, **75**, 817–825.

View Article Online
DOI: 10.1039/C5NJ02604K

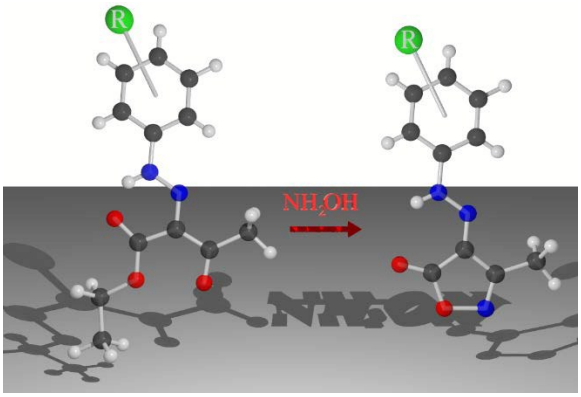

The synthesis and characterization of a family of isoxazolones was performed. X-Ray diffraction over two structures was performed. All compounds showed antineoplastic activity.